Supplementary material

From magnetic order to spin liquid ground states on the S = 3/2 triangular lattice

*J. Tapp, C. R. dela Cruz, M. Bratsch, N.E. Amuneke, L. Postulka, B. Wolf, M. Lang, H.O. Jeschke, R. Valentí, P. Lemmens, and A. Möller**

Table of content:

Supplement references [37-42] are given in the main paper.

(SM-1) Crystallographic data for $RbAg_2Cr[VO_4]_2$

SM-1_Table 1. *Crystal data and refinement for $RbAg_2Cr[VO_4]_2$ (T = 5 K).*

Trigonal, $P\bar{3}$, $Z = 1$	$R_p = 4.68$
$a = 5.44290(4)$ Å	$R_{wp} = 6.61$
$c = 7.3446(1)$ Å	$R_{exp} = 8.23$
$V = 188.43(1)$ Å^3	$R_{Bragg} = 3.01$; $R_f = 2.42$
$\lambda = 2.4062$ Å	$\chi^2 = 0.73$
$2\theta_{min} = 8.50°$, $2\theta_{max} = 129.89°$, $2\theta_{step} = 0.07°$	

SM-1_Table 2. *Fractional atomic coordinates and isotropic displacement parameters for $RbAg_2Cr[VO_4]_2$ (T = 5 K).*

	x	***y***	***z***	B_{iso} (Å^2)
Ag	1/3	2/3	0.2755(6)	0.3(1)
Rb	0	0	0	0.4(2)
Cr	0	0	1/2	0.3(3)
V	1/3	2/3	0.723(2)	0.1(2)
O1	0.6704(7)	0.9143(4)	0.6552(4)	0.67(9)
O2	1/3	2/3	0.9527(5)	0.5(1)

SM-1_Table 3. *Lattice constants for $RbAg_2Cr[VO_4]_2$.*

T (K)	***a (Å)***	***c (Å)***	***V (Å^3)***
293 (XRD)	5.45596(9)	7.3781(3)	190.20(1)
5	5.44290(4)	7.3446(1)	188.43(1)
3	5.44289(4)	7.3444(1)	188.43(1)
2	5.43657(5)	7.3358(1)	187.77(1)
0.26	5.43531(4)	7.3335(1)	187.62(1)

(SM-2) Crystallographic data for $KAg_2Cr[VO_4]_2$

SM-2_Table 1. *Crystal data and refinement for $KAg_2Cr[VO_4]_2$ (T = 293 K).*

Trigonal, $P\bar{3}$, $Z = 1$	$R_p = 4.94$
$a = 5.45796(4)$ Å	$R_{wp} = 6.32$
$c = 7.2384(1)$ Å	$R_{exp} = 5.64$
$V = 186.74(1)$ Å^3	$R_{Bragg} = 6.43$; $R_f = 7.77$
$\lambda = 1.54056$ Å (XRD)	$\chi^2 = 1.96$
$2\theta_{min} = 10.19°$, $2\theta_{max} = 89.97°$, $2\theta_{step} = 0.04°$	

SM-2_Table 2. *Fractional atomic coordinates and isotropic displacement parameters for $KAg_2Cr[VO_4]_2$ (T = 293 K).*

	x	***y***	***z***	B_{iso} (Å^2)
Ag	1/3	2/3	0.2876(7)	0.80(4)
K	0	0	0	0.68(4)
Cr	0	0	1/2	0.63(4)
V	1/3	2/3	0.734(1)	0.48(4)
O1	0.666(2)	0.903(2)	0.662(2)	0.83(4)
O2	1/3	2/3	0.969(1)	0.83(4)

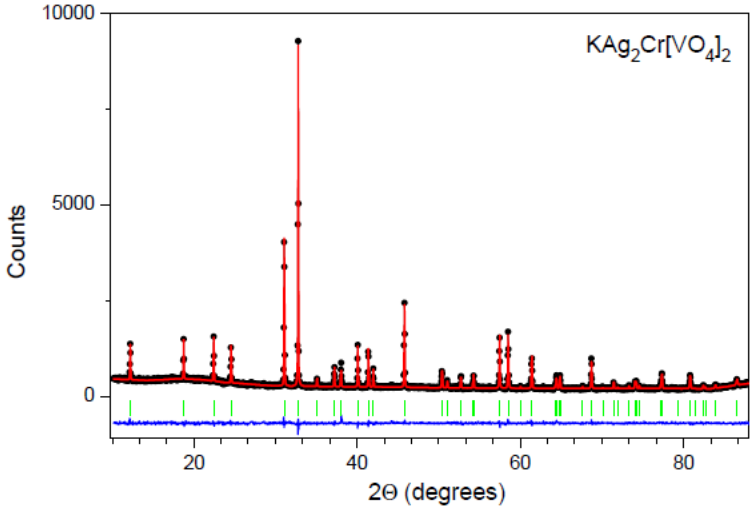

SM-2_Fig. 1. XRD powder pattern refienement: experimental data (*black*), calculated pattern (*red*), difference plot (*blue*), and Bragg positions (*green*).

(SM-3) Crystallographic data for $AgAg_2Cr[VO_4]_2$

SM-3_Table 1. *Crystal data and refinement for $AgAg_2Cr[VO_4]_2$ (T = 2 K).*

Monoclinic, *C*2/*c*, *Z* = 4	Nuclear (magnetic)
a = 9.7094(3) Å	R_p = 5.44
b = 5.0944(2) Å	R_{wp} = 7.97
c = 14.3469(3) Å	R_{exp} = 7.46
β = 93.617(3)°	R_{Bragg} = 5.31 (21.62)
V = 708.22(4) Å^3	R_f = 3.64
λ = 2.4130Å	χ^2 = 1.15
$2\theta_{min}$ = 9.03°, $2\theta_{max}$ = 130.50°, $2\theta_{step}$ = 0.07°	

SM-3_Table 2. *Fractional atomic coordinates and isotropic displacement parameters for $AgAg_2Cr[VO_4]_2$ (T = 2 K).*

	x	***y***	***z***	B_{iso} (Å^2)
Ag1	0	0.036(2)	3/4	0.5(2)
Ag2	0.8416(5)	0.563(1)	0.8580(4)	0.3(2)
Cr1	0	0	1/2	0.4(2)
V1	0.6659(9)	0.039(2)	0.8953(6)	0.3(2)
O1	0.6683(7)	0.882(1)	0.7920(4)	0.8(2)
O2	0.6048(7)	0.823(1)	0.9754(5)	0.7(2)
O3	0.5609(6)	0.310(1)	0.8850(4)	0.8(2)
O4	0.8370(6)	0.127(1)	0.9251(5)	0.8(2)

SM-3_Table 3. *Lattice constants for $AgAg_2Cr[VO_4]_2$.*

T (K)	***a (Å)***	***b (Å)***	***c (Å)***	***β (°)***	***V (Å^3)***
293 (XRD)	9.8108(4)	5.1045(2)	14.3245(5)	93.753(4)	715.82(5)
20	9.7091(3)	5.0933(2)	14.3453(3)	93.631(3)	707.97(3)
2	9.7094(3)	5.0944(2)	14.3469(3)	93.617(3)	708.22(4)

(SM-4) Magnetic part

SM-4_Fig. 1 shows the magnetic susceptibility χ (= dM/dB) of $RbAg_2Cr[VO_4]_2$ as a function of magnetic field B at three different temperatures. At the lowest temperature measured of T = 38 mK, (black circles) the data reveal a pronounced maximum at a field of $B_{max} \approx$ 0.8 T followed by a plateau at intermediate fields of 2.8 T < B < 3.6 T. The strong decrease of χ observed above about $B \approx$ 4.5 T marks the entrance into the fully-polarized state. Upon increasing the temperature to T = 0.28 K (blue circles) the maximum becomes more pronounced and slightly shifts to higher fields ($B_{max} \approx$ 0.9 T). In contrast to the low-temperature data, the curve taken at T = 1.7 K (green circles) displays a monotonic decrease of χ with increasing field without indications for anomalous behavior.

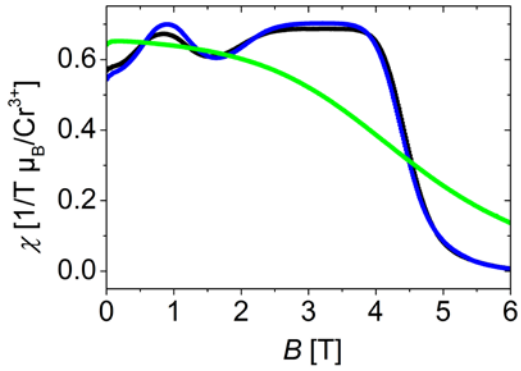

SM-4_Fig. 1. $\chi(B)$ for $RbAg_2Cr[VO_4]_2$ at 38 mK (black), 280 mK (blue), and 1.7 K (green). Data were taken with decreasing field.

SM-4_Fig 2 shows the magnetization M as a function of field B for $RbAg_2Cr[VO_4]_2$ at T = 1.7 K (green circles), measured in a static magnetic field, and $KAg_2Cr[VO_4]_2$ at T = 4.2 K (blue circles), measured in a pulsed field. For $RbAg_2Cr[VO_4]_2$ the fully-polarized state with a total moment of 3 μ_B/Cr^{3+} is reached at a saturation field of $B_s \approx$ 8.5 T. In contrast, saturation is reached for $KAg_2Cr[VO_4]_2$ at much higher fields of about $B_s \approx$ 19 T. This observation is consistent with the distinctly larger coupling constant J for the latter compound, as extracted from the experimentally determined Curie-Weiss temperature and the DFT calculations, presented in the main text. To determine the saturation field in the limit T = 0, $B_s(0)$, we use the crossing points of linear extrapolations as indicated by the dotted lines in SM-4_Fig. 2. This procedure yields $B_s(0) \approx$ 13.5 T for the $KAg_2Cr[VO_4]_2$ compound and $B_s(0) \approx$ 5 T for $RbAg_2Cr[VO_4]_2$. The latter value is in a good agreement with B_s determined from low-temperature (T = 0.038 K) measurements shown in the main text.

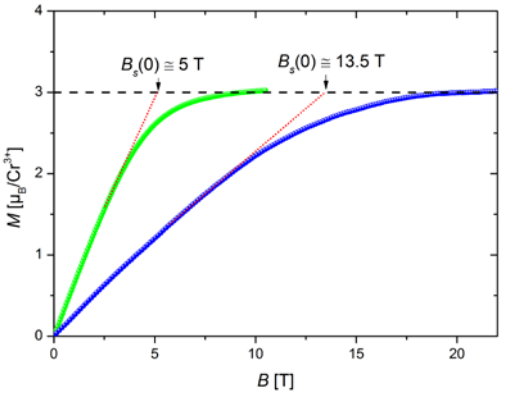

SM-4_Fig. 2. Magnetization for $RbAg_2Cr[VO_4]_2$ (green) measured at T = 1.7 K and $KAg_2Cr[VO_4]_2$ (blue) measured at T = 4.2 K .

(SM-4) Magnetic part – continued

SM-4_Fig. 3 shows the temperature derivative of χ as a function of temperature for $RbAg_2Cr[VO_4]_2$ (a) and $KAg_2Cr[VO_4]_2$ (b). For $RbAg_2Cr[VO_4]_2$ we find a pronounced maximum in $d\chi/dT$ at $T_{max} \approx 0.57$ K for zero field (red circles) and at about 0.53 K at a small field of $B = 0.1$ T (orange circles). On increasing the field to $B = 0.5$ T and 1 T, the maximum becomes blurred. Note that in this intermediate field range, an anomaly is observed in field-dependent susceptibility measurements, accompanied by hysteretic behavior (see main text), which we assign to a field-induced ordered state. On further increasing the field to $B \geq 1.5$ T, where no such anomaly is detected in the field-dependent susceptibility measurements, however, the maximum is recovered, although somewhat reduced in size and slightly shifted to lower temperatures.

According to *Ramirez* et al. [Ref. 37], such an extremum in $d\chi/dT$ and a crossing point of the various $C_m(T, B)$ curves around 1 K (see main text), are signatures for the crossover from a high-temperature paramagnetic state into a low-temperature spin liquid phase.

A similar scenario is also observed for $KAg_2Cr[VO_4]_2$ (b). Here we find that the extremal position in $d\chi/dT$ barely changes with the magnetic field. Note that around the same temperature of about 3 K, the specific heat curves taken in various fields cross in a single point, see main text.

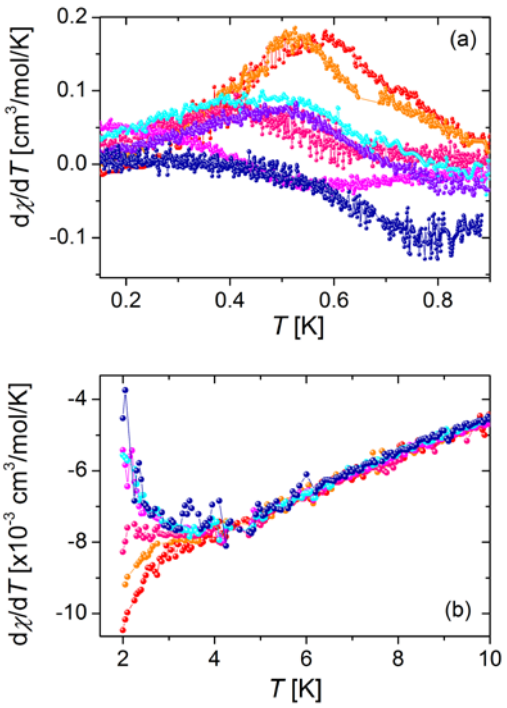

SM-4_Fig. 3. Temperature derivative of χ for $RbAg_2Cr[VO_4]_2$ (a) and $KAg_2Cr[VO_4]_2$ (b). The data are taken at various magnetic fields. *Top* (a): red 0 T; orange 0.1 T; pink 0.5 T; magenta 1.0 T; cyan 1.5T ; violet 2.0 T; dark blue 3.0 T. *Bottom* (b): red 0.1 T; orange 1.0 T; pink 2.0 T; magenta 3.0 T; cyan 4.0 T; violet 2.0 T; dark blue 3.0 T.

(SM-5) Ab-initio calculations

We perform density functional theory calculations with the full potential local orbital (FPLO) method [Ref. 38] and generalized gradient approximation exchange correlation functional [Ref. 39]. We account for strong correlations on Cr 3*d* with a GGA+U correction [Ref. 40]. We fix the Hund's rule coupling J_H to 0.72 eV as suggested in Ref. 41. Theoretical values of the isotropic exchange couplings are obtained by mapping total energies of different spin configurations onto the Heisenberg Hamiltonian [Ref. 42]. For this purpose, we constructed 3×2×1 supercells with *P*1 symmetry in the case of $KAg_2Cr[VO_4]_2$ and $RbAg_2Cr[VO_4]_2$, respectively, and 2×2×1 supercells with $P\ \bar{1}$ symmetry for $AgAg_2Cr[VO_4]_2$ based on the crystallographic data, see above. This allows us to extract the exchange couplings listed in SM-5_Table 1.

For $Ag_3Cr[VO_4]_2$ we find an anisotropic triangular lattice (see SM-5_Fig. 1 (a)), with one-dimensional J_1 chain couplings about 63% of the nearly isotropic square lattice formed by J_{2a} and J_{2b}. Note that while J_{2a} and J_{2b} belong to the same Cr-Cr distance of 5.47 Å, they slightly differ in the orientation of the $[VO_4]$ tetrahedra mediating the coupling. This leads to about 1% difference between J_{2a} and J_{2b}. We find that interlayer couplings are nearly negligible at around 1% of the largest coupling.

In contrast, $KAg_2Cr[VO_4]_2$ and $RbAg_2Cr[VO_4]_2$ are characterized by a perfect triangular lattice with nearly negligible second neighbor coupling in the plane (see SM-5_Fig. 1 (b)). Here substantial antiferromagnetic interlayer coupling of 11% and 9% of the largest coupling exists.

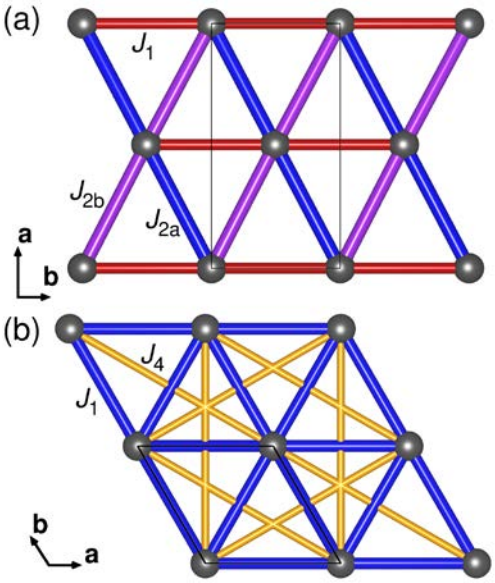

SM-5_Fig. 1: Geometry of the inter-layer exchange couplings for (a) $Ag_3Cr[VO_4]_2$ and (b) $KAg_2Cr[VO_4]_2$ and $RbAg_2Cr[VO_4]_2$. In (a) two second nearest neighbors are at the same distance but differ in $[VO_4]$ tetrahedron orientation (not shown). Note, that the index *i* of the J_i enumerates with increasing Cr-Cr distances.

(SM-5) Ab-initio calculations - continued

SM-5_Table 1. Calculated exchange couplings (in Kelvin) for $AAg_2Cr[VO_4]_2$ (A = Ag, K, Rb). The geometry of the intra-plane couplings is illustrated in SM-5-Fig. 1. The interaction strength U = 2 eV for A = Ag and U = 1 eV for A = K, Rb is chosen by demanding that the mean field Curie-Weiss temperature matches the experiment.

A	***intra-plane couplings (K)***			***inter-layer couplings (K)***		
Ag	J_1 = 2.98(1)	J_{2a} = 4.69(1)	J_{2b} = 4.74(1)	J_3 = -0.062(1)	J_4 = -0.006(1)	J_5 = -0.028(1)
Rb	J_1 = 0.427(3)	J_4 = 0.011(2)		J_2 = 0.046(3)		
K	J_1 = 2.81(1)	J_4 = -0.009(3)		J_2 = 0.261(4)		